Supporting Information for "Kinematics of footwall exhumation at oceanic detachment faults: solid-block rotation and apparent unbending"

Dan Sandiford[1,2], Sascha Brune[2,3], Anne Glerum[2], John Naliboff[4], Joanne M. Whittaker[1]

[1]Institute for Marine and Antarctic Studies, University of Tasmania, Hobart, Tasmania, Australia, 7004

[2]Helmholtz Centre Potsdam - German Research Centre for Geosciences (GFZ)

[3]Institute of Geosciences, University of Potsdam, Potsdam, Germany

[4]Department of Earth and Environmental Science, New Mexico Institute of Mining and Technology

Contents of this file

1. Text S1 to S2
2. Figure S1
3. Table S1

Additional Supporting Information (Files uploaded separately)

1. Captions for Movies S1 and S2
2. ASPECT parameter (.prm) file

Text S1: TAG seismicity

Fig. S1 shows map and cross-section views of the hypocenters from the Trans-Atlantic Geotraverse (TAG) detachment at the Mid-Atlantic Ridge, produced by Demartin et al. (2007). That study identified two distinct zones of seismic activity, one interpreted to represent the curved trace of the active detachment fault, and a second locus about 8 km outboard of the detachment cluster, suggested to relate to antithetic normal fault planes in the footwall. It is notable that microseismicity along the detachment is concentrated some 2-7 km beneath the seafloor. Craig and Parnell-Turner (2017) argue that the shallowest part of the TAG detachment (also the least-optimally oriented) tends to produce larger-magnitude earthquakes, and less microseismicity.

In map view, the TAG epicenters form a donut shape, with a prominent seismic gap in the footwall adjacent to the detachment fault termination at the seafloor. Focal mechanisms shown in Fig. S1 are representative, constructed from the dip values referred to in Demartin et al. (2007). Readers are referred to the original study for further details. In the manuscript (Fig. 3) the earthquakes plotted are those within a distance $\pm$ 4.5 km from the line A-A', which attempts to minimise the 3-D aspects of the full seismicity pattern.

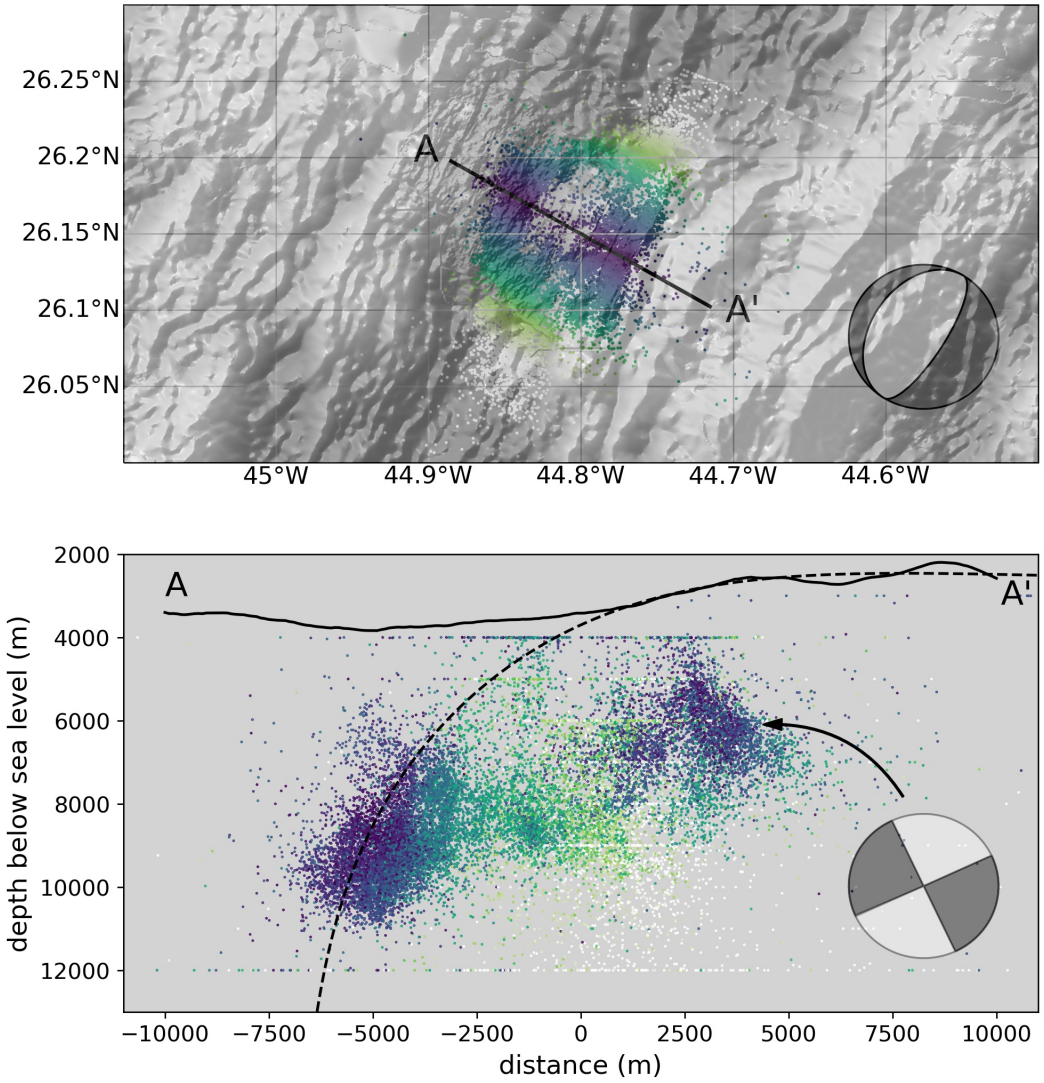

Figure S1. Hypocenters from the TAG detachment segment of the the Mid-Atlantic Ridge, from the study of Demartin et al. (2007). The distance of line between A-A' in the top panel is 20 km. Hypocenters are coloured to show relative distance from the line. Bottom panel shows a cross sectional view of the seismicity. The dashed line is a parameterization of the emergent detachment morphology from our numerical model.

Text S2: Numerical model methods

Thermo-mechanical model

We model the 2-D thermo-mechanical evolution of an amagmatic oceanic spreading center, using ASPECT to solve the incompressible Stokes and advection-diffusion equations, according to the Boussinesq approximations described in Bangerth et al. (2020b). Adiabatic and shear heating are thus neglected in the energy equation. Elastic shear deformation is included in the constitutive model, necessitating an additional force term in the Stokes equations (e.g. Schmalholz et al. (2001); Moresi et al. (2003); Bangerth et al. (2020)). There is no compositional differentiation in the model (e.g. crust versus mantle) and the constitutive model applies to all parts of the domain. The temperature dependence of the dislocation creep means that creep increasingly dominates at temperatures $\geq 600°\mathrm{C}$, while colder parts of lithosphere are effectively elasto-brittle. The constitutive model is described in the following section.

Viscous creep

The effective viscosity associated with high temperature dislocation creep is modelled with a wet olivine flow law (Hirth & Kohlstedt, 2003):

$$\eta = \frac{1}{2} A^{-\frac{1}{n}} |D|^{\frac{1-n}{n}} \exp\left(\frac{E + p\,V}{nRT}\right) \tag{1}$$

$|D|$ is the square root of the second invariant (or magnitude) of the deviatoric strain rate tensor: $|D| = (D_{ij} D_{ij}/2)^{1/2}$. R is the gas constant, T is temperature, p is pressure, A is the prefactor, n is the stress exponent, E is the activation energy and V is the activation volume. Values are provided in Table S1.

The prefactor A is weakened linearly with accumulated viscous strain, following the same functional form as the brittle strength weakening (e.g. Eqn. 11, see also Naliboff et al. (2020)). Relevant parameters are given in Table S1.

Visco-elasticity

This section describes the implementation of Maxwell visco-elasticity within a Stokes flow framework, where the stress history is tracked in an Eulerian reference frame (as

in ASPECT 2.2.0). Compared with a Lagrangian tracking scheme, such as described by Moresi et al. (2003), the key difference is that advective terms must be accounted for in the stress rate tensor.

In the Maxwell viscoelastic model, strain rates are proportional to the sum of the stress and stress rate. D_{ij}, is given by

$$D_{ij} = D^v_{ij} + D^e_{ij} = \frac{\tau_{ij}}{2\eta} + \frac{1}{2\mu}\frac{D\tau_{ij}}{Dt}. \tag{2}$$

Where τ_{ij} is the deviatoric part of the Cauchy stress tensor. To simplify the description in this section, we use η to refer to viscosity associated with dislocation creep (i.e. $\eta = \eta(T, p, |D|)$).

The constitutive relationship for a Maxwell viscoelastic fluid (Eqn. 2) contains the stress rate tensor. The temporal derivative in the stress rate is a material derivative and, as we will track the stress rate in a Eulerian reference frame, advective terms must be accounted for.

A further requirement is that the stress rate tensor remains objective to rotation experienced by the material parcels (see Schmalholz et al. (2001); R. J. Farrington (2017) for details). This problem is typically handled by adopting an objective stress rate, in order to enforce the objectivity. Following (Moresi et al., 2003), we employ the Zaremba-Jaumann definition of stress rate:

$$\frac{D\tau_{ij}}{Dt} = \frac{\partial\tau_{ij}}{\partial t} + v_k\frac{\partial\tau_{ij}}{\partial x_k} - W_{ik}\tau_{kj} + \tau_{ik}W_{kj} \tag{3}$$

where W is the spin tensor.

Following Schmalholz et al. (2001); Moresi et al. (2003), ASPECT 2.2.0 discretizes the temporal part of $\frac{D\tau_{ij}}{Dt}$ using backwards finite difference:

$$\frac{\partial\tau^t_{ij}}{\partial t} \approx \frac{\tau^t_{ij} - \tau^{t-\Delta t}_{ij}}{\Delta t}$$

(4)

Solving for τ^t:

$$
\begin{aligned}
D_{ij}^t &= \frac{1}{2\eta}\tau_{ij}^t + \frac{1}{2\mu}\left(\frac{\tau_{ij}^t}{\Delta t} - \frac{\tau_{ij}^{t-\Delta t}}{\Delta t} + v_k\frac{\partial \tau_{ij}^{t-\Delta t}}{\partial x_k} - W_{ik}\tau_{kj}^{t-\Delta t} + \tau_{ik}^{t-\Delta t}W_{kj}\right) \\
\left(\frac{\mu\Delta t}{\mu\Delta t\eta} + \frac{\eta}{\mu\Delta t\eta}\right)\tau_{ij}^t &= 2D_{ij}^t + \frac{1}{\mu}\left(\frac{\tau_{ij}^{t-\Delta t}}{\Delta t} + v_k\frac{\partial \tau_{ij}^{t-\Delta t}}{\partial x_k} - W_{ik}\tau_{kj}^{t-\Delta t} + \tau_{ik}^{t-\Delta t}W_{kj}\right) \\
\tau_{ij}^t &= \left(\frac{\mu\Delta t\eta}{\mu\Delta t + \eta}\right)\left(2D_{ij}^t + \frac{1}{\mu}\left(\frac{\tau_{ij}^{t-\Delta t}}{\Delta t} + v_k\frac{\partial \tau_{ij}^{t-\Delta t}}{\partial x_k} - W_{ik}\tau_{kj}^{t-\Delta t} + \tau_{ik}^{t-\Delta t}W_{kj}\right)\right) \\
\tau_{ij}^t &= \eta_{\text{eff}}\left(2D_{ij}^t + \frac{1}{\mu}\left(\frac{\tau_{ij}^{t-\Delta t}}{\Delta t} + v_k\frac{\partial \tau_{ij}^{t-\Delta t}}{\partial x_k} - W_{ik}\tau_{kj}^{t-\Delta t} + \tau_{ik}^{t-\Delta t}W_{kj}\right)\right)
\end{aligned}
$$

For brevity, define $\tilde{\tau}_{ij}$ as the stress history tensor advected and rotated into the configuration of the current timestep:

$$
\tilde{\tau}_{ij} = \left(\tau_{ij}^{t-\Delta t} + v_k\frac{\partial \tau_{ij}^{t-\Delta t}}{\partial x_k} - W_{ik}\tau_{kj}^{t-\Delta t} + \tau_{ik}^{t-\Delta t}W_{kj}\right) \tag{5}
$$

so that

The stress at timestep t is given by:

$$
\tau^t = \eta_{\text{eff}}\left(2D_{ij}^t + \frac{1}{\mu\Delta t}\tilde{\tau}_{ij}\right) \tag{6}
$$

The Stokes Equation, representing conservation of momentum at infinite Prandtl number, can then be modified as follows:

$$
(2\eta_{\text{eff}}D_{ij})_{,j} - p_{,i} = f_i - \frac{\eta_{\text{eff}}}{\mu\Delta t}\tilde{\tau}_{ij,j} \tag{7}
$$

Advection and rotation terms in the stress rate

In ASPECT v2.2.0 (Bangerth et al., 2020), the stress history tensor is stored (component wise) as a set of non-diffusive scalar compositional fields. In the current imple-

mentation a two-stage approach is used to approximate the Zaremba-Jaumann stress rate. The advection terms for each component of stress rate are handled by the ASPECT's default compositional field capability. Version 2.2.0 of ASPECT uses a 2nd order implicit time integration for the advection equations (BDF-2).

Whenever the components of the stress history tensor are accessed (e.g. by various ASPECT material models) the relevant advection terms for each component will already have been calculated. The rotation terms in the Zaremba-Jaumann stress rate are then applied in the 'elasticity' submodule (`aspect/source/material_model/rheology/elasticity.cc`):

$$\tilde{\tau}_{ij}^{t} = \frac{1}{\mu}\left(\frac{\check{\tau}_{ij}^{t}}{\Delta t} - W_{ik}\check{\tau}_{kj}^{t} + \check{\tau}_{ik}^{t}W_{kj}\right) \tag{8}$$

Where $\check{\tau}_{ij}^{t}$ refers to the stress history tensor after advective terms have been handled.

At the completion of the Stokes solve and the progression to the next time step, the components of the stress history tensor need to be updated. This process is also handled using ASPECT's compositional field capability. The update increment to the stress history components are applied as a 'reaction term', i.e. a source term in the advection equation.

Following R. Farrington et al. (2014), instead of simply taking the stress history at $t-1$, we store the stress history term $\check{\tau}$ as a running average ($\bar{\tau}_{ij}$) defined as:

$$\bar{\tau}_{ij} = (1-\Phi)\tilde{\tau}_{ij} + \Phi\tau ij \tag{9}$$

where $\Phi = \Delta t_c/\Delta t_e < 1$.

Visco-elasto-plastic model

Plastic deformation is incorporated into the visco-elastic constitutive model, following Moresi et al. (2003). Brittle behaviour is modelled through a Drucker-Prager yield limit (τ_y) on the magnitude of the deviatoric stress:

$$\tau_y = p\,sin(\phi) + Ccos(\phi) \tag{10}$$

where p is the pressure. The cohesion (C) and friction angle (ϕ) are weakened with accumulated plastic strain (γ^p) according to:

$$C(\beta) = \beta C_1 + (1 - \beta)C_0 \tag{11}$$

Where

$$\beta = min(1, \gamma^p / \gamma_0^c) \tag{12}$$

The model is initialised with plastic strain on the quadrature points, randomly sampled from a uniform distribution between 0 and 0.25.

Again we use the notation $\tilde{\tau}$ (omitting component indexes here for brevity) for the stress history tensor (advected and rotated into the configuration of the current timestep). Define an effective strain rate as:

$$D_{\text{eff}} = 2D + \frac{1}{\mu \Delta t_e} \tilde{\tau} \tag{13}$$

with the magnitude given by: $|D| = (D_{ij} D_{ij}/2)^{1/2}$. The plastic effective viscosity is then defined as:

$$\eta_{\text{p}} = \frac{\tau_y}{|D_{\text{eff}}|} \tag{14}$$

Substituting (14) into the definition of the stress (Eqn. 6) shows that this definition of the plastic viscosity satisfies the yield stress (i.e. it produces the intended viscosity rescaling at each iteration).

The final viscosity η_{vep} is defined depending on whether the magnitude of the deviatoric stress tensor exceeds τ_y^t:

$$\eta_{\text{vep}} = \begin{cases} \eta_{\text{p}}, & |\tau^t| \geq \tau_y \\ \eta_{\text{eff}}, & \text{otherwise} \end{cases}$$

A successive substitution (Picard) approach is used to resolve the nonlinearity in the material model. The maximum number of iterations is limited to 40.

128 ## Model parameters

Parameter name	**Value**	**Symbol**	**Units**
Model domain depth	100	-	km
Model domain width	400	-	km
Potential temperature	1573	T_p	K
Surface temperature	293	T_s	K
Viscosity minimum	1×10^{18}	-	Pa s
Viscosity maximum	1×10^{24}	-	Pa s
Dislocation creep volume	22×10^{-6}	V	$m^3\,mol^{-1}$
Dislocation creep energy	520	E	$kJ\,mol^{-1}$
Dislocation creep exponent	3.5	n	-
Initial dislocation creep prefactor	3.77×10^{-14}	A_0	$Pa^{-n}\,s^{-1}$
Weakened dislocation creep prefactor	1.385×10^{-14}	A_1	$Pa^{-n}\,s^{-1}$
Prefactor weakening interval	2	γ_0^A	-
Initial friction angle	30	ϕ_0	$^\circ$
Initial cohesion	20	C_0	MPa
Weakened friction angle	3	ϕ_1	-
Weakened cohesion	10	C_1	MPa
Friction angle weakening interval	6	γ_0^ϕ	-
Cohesion weakening interval	6	γ_0^C	-
Elastic shear moduli	10	μ	GPa
Thermal diffusivity	3×10^{-6}	-	km
Heat capacity	1000	C_p	$J\,K^{-1}\,kg^{-1}$
Full spreading rate	2	-	$cm\,yr^{-1}$
Elastic timestep	10^4	Δt_e	yr
Numerical timestep (max)	2×10^3	Δt_c	yr
Reference density	3300	ρ_0	$kg\,m^{-3}$
Thermal expansivity	3.5×10^{-5}	α	K^{-1}

Table S1. Parameters used in the reference model. See also the included ASPECT input file (`input_reference_model.prm`). The alternative model differs only in that $\gamma_0^\phi = \gamma_0^C = 2$.

Movie S1 and S2 Captions

Movie S1 shows evolution of the reference model. The top panel shows the horizontal component (D_{xx}) of the strain rate tensor for the reference model, at times labelled. The model velocity field is shown with arrows. The bottom panel shows the vorticity, along with the accumulated plastic strain in greyscale, saturated at a value of 0.7. Bottom panel also shows vectors of the translated velocity field (velocity in the hanging wall reference frame). The two black lines in each panel show contours of the temperature field at 600 and 700 °C.

Movie S2 shows evolution of alternative model, where the strain intervals that determine plastic strength weakening are reduced. All features shown are identical to Movie S1.

References

Bangerth, W., Dannberg, J., Gassmoeller, R., & Heister, T. (2020, June). *Aspect v2.2.0.* Zenodo. Retrieved from https://doi.org/10.5281/zenodo.3924604 doi: 10.5281/zenodo.3924604

Bangerth, W., Dannberg, J., Gassmöller, R., Heister, T., et al. (2020b, June). ASPECT: Advanced Solver for Problems in Earth's ConvecTion, User Manual. Retrieved from https://doi.org/10.6084/m9.figshare.4865333 (doi:10.6084/m9.figshare.4865333) doi: 10.6084/m9.figshare.4865333

Craig, T. J., & Parnell-Turner, R. (2017). Depth-varying seismogenesis on an oceanic detachment fault at 13 20 n on the mid-atlantic ridge. *Earth and Planetary Science Letters*, *479*, 60–70.

Demartin, B. J., Sohn, R. A., Canales, J. P., & Humphris, S. E. (2007). Kinematics and geometry of active detachment faulting beneath the trans-atlantic geotraverse (tag) hydrothermal field on the mid-atlantic ridge. *Geology*, *35*(8), 711–714.

Farrington, R., Moresi, L.-N., & Capitanio, F. A. (2014). The role of viscoelasticity in subducting plates. *Geochemistry, Geophysics, Geosystems*, *15*(11), 4291–4304.

Farrington, R. J. (2017, 10). Geodynamic models of lithospheric and mantle processes. Retrieved from https://bridges.monash.edu/articles/thesis/Geodynamic_models_of_lithospheric_and_mantle_processes_/4644928 doi: 10.4225/03/58a158e99e4df

Hirth, G., & Kohlstedt, D. (2003). Rheology of the upper mantle and the mantle wedge: A view from the experimentalists. *Geophysical Monograph-American Geophysical Union*, *138*, 83–106.

Moresi, L., Dufour, F., & Mühlhaus, H.-B. (2003). A lagrangian integration point finite element method for large deformation modeling of viscoelastic geomaterials. *Journal of computational physics*, *184*(2), 476–497.

Naliboff, J., Glerum, A., Brune, S., Péron-Pinvidic, G., & Wrona, T. (2020). Development of 3-d rift heterogeneity through fault network evolution. *Geophysical Research Letters*, *47*(13), e2019GL086611.

Schmalholz, S., Podladchikov, Y., & Schmid, D. (2001). A spectral/finite difference method for simulating large deformations of heterogeneous, viscoelastic materials. *Geophysical Journal International*, *145*(1), 199–208.